Supplementary material for:

Astroglial noradrenaline shapes cerebellar synaptic integration and motor adaptation

Sambre Mach, Juliette Royer, Wenli Niu, Xia Li, Rafael Benzi, Nathalie Desvignes, Julien Bouvier, Micaela Galante*✉ & Glenn Dallérac*✉

Institut des Neurosciences Paris-Saclay, Université Paris-Saclay, CNRS UMR9197, 91400, Saclay, France.

* Equal contribution

✉ glenn.dallerac@cnrs.fr, micaela.galante@universite-paris-saclay.fr

Materials and Methods

Animal models

Experiments were conducted on male and female mice between postnatal day 60 (P60) and P90, in accordance with the European Community Council Directives of 1 January 2013 (2010/63/EU) and with the approval of the local animal welfare committee (certificate B 91 272 108). Animals were housed in a temperature-controlled environment (25 °C) under a 12 h light/dark cycle. All mouse lines were maintained on a C57BL/6J genetic background. When no sex differences were observed, data from male and female mice were pooled for analysis. Several transgenic lines were used in this study. The ALDH1L1-EGFP line expresses the enhanced green fluorescent protein (EGFP) under the control of the astrocyte-specific Aldh1l1 promoter. The aVMAT2cKO mice were kindly provided by Paola Bezzi (University of Lausanne) and generated by crossing the GFAPcre^{ERT2} line expressing a tamoxifen (TAM) inducible cre recombinase transgene driven by the astrocytic glial fibrillary acidic protein (GFAP) promoter with the VMAT2$^{lox/lox}$ line containing cre-excisable loxP sequences in the endogenous VMAT2 [1,2]. Recombination was induced by intraperitoneal injections of tamoxifen (100 mg/kg) for five consecutive days, animals were used after a minimum of 10 days after the first injection. Finally, DBH-cre mice were kindly gifted by Bruno Giros (Paris Cité University) and express the cre recombinase transgene under the dopamine-beta-hydroxylase (DBH) promoter.

Immunohistochemistry

Mice were deeply anesthetized with Dolethal and transcardially perfused with iced-cold buffered saline (PBS) for exsanguination and with a 4% paraformaldehyde in PSB solution for fixation composed of (in mM): 35.4 NaH_2PO_4*2H_2O, 160.7 Na_2HPO_4*2 H_2O, 154 NaCl, pH 7.4. Brains were removed and post-fixed overnight at 4°C, then equilibrated with 30% sucrose at 4°C and frozen for storage at -20°C until immunohistochemistry. Sagittal 35µm thick cerebellar slices were collected using a cryostat. Brain slices were washed with PBS, permeabilized with 0.5% Triton X-100 and labeled with primary antibodies overnight at 4°C. Primary antibodies included: rabbit anti-VMAT2 (1/500, Synaptic Systems), rabbit anti-OCT3 (1/500, Gentaur), mouse anti-NET (1/500, ALOMONE AMT-002), rabbit anti-DAT (1/500, ABCAM AB184451), rabbit anti-DBH (1/500, ABCAM AB209487), mouse anti-calbindin (1/1000; Merck C9848), mouse anti-GS (1/500, Merck MABN543), rabbit anti-TH (1/500, ABCAM AB152), mouse anti-COMT (1/400, BD Biosciences #611970). Following primary antibody incubation, slices were washed twice with PBS before incubation with the appropriate secondary antibody for 2h at room temperature with the following secondary antibodies: goat anti-rabbit 555 (1/1000, Thermofischer Scientific #A-21428), goat anti-mouse 488 (1/1000, Thermofischer Scientific

#A-11001), goat anti-rabbit 647 (1/1000, Thermofischer Scientific #A-21245). Slices were then washed twice with PBS and once with PB (in mM: 35.4 NaH_2PO_4*$2H_2O$, 160.7 Na_2HPO_4*2 H_2O) before being mounted in fluoromount (Thermoficher Scientific #18744094). Slices were observed under a confocal Leica SP8 microscope with x10 (0.4 NA), x25 (0.95 NA) and x40 (1.3 NA) objectives. Images were acquired at 12 bit with identical laser power and PMT settings and analyzed with ImageJ and LasX softwares. NE staining (1/500, Immusmol #IS1028) was performed using the STAINperfect Immunostaining kit (ImmuSmol #SP-A-1000, Bordeaux, France), following the manufacturer's protocol: mice were anesthetized and transcardially perfused with a combination of ice-cold 2% paraformaldehyde and the ImmuSmol fixation solution. Coronal and sagittal 35µm slices were collected with a cryostat (free-floating) and immunostaining was performed according to ImmuSmol protocol. Immunostainings were quantified as the proportion of cells identified by Purkinje cell or astrocytic markers that expressed the target protein.

Magnetic-activated cell sorting (MACS) isolation of astrocytes

Mice were deeply anesthetized with isoflurane and euthanized by cervical dislocation. The cerebellar vermis was rapidly dissected for astrocyte isolation and enzymatically dissociated at 37 °C for 30 minutes with the Miltenyi Adult Brain Dissociation Kit (130-107-677, Miltenyi Biotech, France) with gentle trituration every 10 minutes to obtain a single-cell suspension. After filtration through a through a 70 µm SmartStrainer, cells were pelleted by centrifugation (300 × g, 10 minutes, 4 °C) and resuspended in PBS + 0.5 % BSA. Fc receptors were blocked with the accompanying FcR Blocking Reagent, then cells were labeled with Anti-ACSA-2 MicroBeads (130-097-678, Miltenyi Biotech, France) for 15 minutes at 4 °C and loaded onto magnetic selection (MS) columns for positive selection. MS columns were washed twice with PBS + 0.5 % BSA and ACSA-2^+ astrocytes eluted in 500 µL sorting buffer. For each genotype (WT and aVMAT2cKO), astrocytes isolated from five mice were pooled, counted on an automated cell counter (DeNovix, France), and pelleted by centrifugation (300 x g, 5 minutes).

Protein quantification by automated capillary immunoassay

Cell pellets obtained with the MACS isolation of astrocytes were lysed in 100 µL buffer containing protease and phosphatase inhibitors. Lysates were then incubated on ice for 20 minutes with intermittent mixing and cleared by centrifugation (5000 × g, 15 min, 4 °C). Protein concentrations were determined by Bradford assay (Bio-Rad). Capillary immunoassays were then performed with an "automated western blot system" (WES, ProteinSimple, BioTechne) using the 12-230 kDa Separation Module combined to either the anti-rabbit (#DM-001) or anti-mouse (#DM-00) detection modules depending on the primary antibody. This automated capillary immunodetection delivers antibody-based separation and quantification equivalent to a classical Western blot, with improved throughput and precision. Protein concentration in supernatants of isolated astrocytes was first determined by Bradford assay (Bio-Rad), adjusted to 1 µg/ml in sample buffer provided in the separation module and processed according to the protocol provided by the manufacturer. A six point calibration curve was included to determine the optimal antibody concentration for reliable and quantitative detection. Data analysis was performed using the SimpleWes software, by verifying molecular-weight markers and peak assignment. The area under the curve (AUC) for each peak was exported in excel for subsequent statistical analysis.

Surgery

Stereotaxic injections of AAVs

Mice anesthesia was induced with 4% isoflurane in 100% O_2, and maintained with 1-1.5% isoflurane. Body temperature was monitored and maintained at 37°C during the whole procedure. The scalp was shaved and sterilized with betadine and 70% alcohol before an incision was made followed by drilling to access the skull. Intracerebral injections were achieved using a glass pipette connected to

a syringe pump (Legato 130, KD Scientific). Viruses were delivered at a rate of 0.05-0.1 µL/min. Virus capillary was slowly removed after three minutes post-injection.

For the combined expression of the $GRAB_{NE2h}$ sensor and the excitatory DREADD in WT mice, 500 nL of AAV9-hSyn-$GRAB_{NE2h}$-GFP (WZ Biosciences Inc, $2.76x10^{13}$ GC/ml) and 500 nL AAV5-GFAP-hM3Dq-mCherry (Addgene, #50478, $1.8x10^{13}$ GC/ml) viruses were injected in lobule VI of the cerebellum (AP: -6.96 mm, ML: 0.0 mm, DV: −0.40 mm). AAV8-Pcp2-hM3Dq-mCherry viral vectors (> $4.0x10^{13}$ GC/ml) allowing specific excitatory hM3Dq expression in PC were provided by Viral Vector Core (University of Minnesota) and co-injected with the $GRAB_{NE2h}$ sensor mentioned above following the same protocol. DBH-Cre mice were bilaterally injected with 200 nL of AAV9-hSyn-DIO-hM4D(Gi)-mCherry (Addgene, #44362, $2.5x10^{13}$ GC/ml) viral vectors in the LC (AP: -5.45 mm, ML: = +/-0.85 mm, DV = −3.65 mm) for expression of hM4Di DREADD in NE neurons. CalEx viruses (AAV5-gfaABC1D-mCherry-hPMCA2w/b, Addgene #111568, $8.9x10^{12}$ GC/ml) were co-injected with GFAP-hM3Dq and either GCaMP6f (AAV5-gfaABC1D-lck-GCaMP6f, Addgene #52924, $2.5x10^{13}$ GC/ml) or $GRAB_{NE2h}$ in a total volume of 1 µL. All animals were used 3 to 4 weeks after injection.

Cranial window and baseplate implantation

For in vivo imaging, a 3 mm diameter circular craniotomy was made above the cerebellar vermis (AP: −6.5 to −7.0 mm; ML: 0.0 mm from Bregma). Three injections of $GRAB_{NE2h}$ virus (300 nL each) in the vermis were performed before the craniotomy was sealed with a sterile glass coverslip (3 mm diameter, #1 thickness), fixed using surgical glue and by dental cement. Mice were allowed to recover for one week. Subsequently, a miniscope-compatible baseplate (Inscopix) was implanted above the cranial window using dental cement to allow miniscope fixation. Mice were then allowed to recover for an additional 2 weeks before starting imaging sessions.

Preparation of ex vivo cerebellar slices

Mice at P60-P80 were deeply anesthetized with isoflurane and sacrificed. The cerebellar vermis was collected after removal of the brain and placed in cold (4°C), oxygenated (95% O2 + 5% CO2) cutting artificial cerebrospinal fluid (cutting ACSF, in mM: 110 NaCl, 5 KCl, 2.5 $CaCl_2$, 1.5 $MgSO_4$, 1.24 KH_2PO_4, 10 D-glucose, 27.4 $NaHCO_3$, 0.05 D-AP5). The vermis was then sagitally cut at 250 µM using a vibrating blade microtome (650HV, Microm France) for whole-cell patch clamp recordings, and at 400 µM for two-photon imaging. Slices were then transferred to room temperature recording ACSF (in mM: 110 NaCl, 5 KCl, 2.5 $CaCl_2$, 1.5 $MgSO_4$, 1.24 KH_2PO_4, 10 D-glucose, 27.4 $NaHCO_3$) and allowed to recover for 1h prior to recordings.

Electrophysiological recordings

Individual slices were transferred to a submerged chamber mounted on a fixed-stage Scientifica SliceScope Pro 1000 electrophysiology microscope. Slices were continuously perfused with oxygenated ACSF maintained at 30-32°C with a temperature controller managed by the LinLab software (Scientifica), with a flow rate of 2mL/min. Signals were acquired with a MultiClamp 700B amplifier (Molecular Devices) filtered at 1 kHz and recordings were obtained with the Clampex software (Molecular Devices, UK). Spontaneous excitatory and inhibitory postsynaptic currents (sEPSCs and sIPSCs) were recorded from PC by whole-cell patch clamp using borosilicate glass capillaries (Harvard Apparatus,1.5 OD x 0.86 ID x 100L) with a resistance of 4-5 MΩ, filled with the following intracellular solution in mM: 144 potassium gluconate, 1 $MgCl_2$, 10 HEPES, 0.5 EGTA (pH 7.4, 280 mOsm). Cells with an access resistance > 20 MΩ at resting potential were excluded from analyses as well as any cell for which a >20 % change in those parameters occurred during the course of the experiment. PC were recorded in voltage-clamp mode with a holding potential of -60 mV. Spontaneous inhibitory post-synaptic currents (sIPSCs) were recorded in the presence of the AMPA receptor antagonist NBQX (10 µM, HelloBio #HB0443) and the NMDA receptor antagonist D-AP5 (50 µM, HelloBio #HB0225) while

spontaneous excitatory post-synaptic currents (sEPSCs) were recorded in the presence of the $GABA_A$ receptor antagonist gabazine (5 µM, HelloBio #HB0901). Spontaneous currents were analyzed with Easy Electrophysiology software (Easy Electrophysiology Ltd, UK).

Pharmacological block of noradrenergic receptors was obtained by the application of antagonists prazosin (α1, Merck #P7791-50MG, 30 µM), propranolol (β, Merck # P0884-1G,10 µM), and phentolamine (α, Merck # P7547-100MG, 30 µM). For experiments with mice expressing DREADD, clozapine N-oxyde (CNO, Sigma-Aldrich #SML2304, 10 µM) was added to the bath solution.

In experiments using mice injected with AAV8-Pcp2-hM3Dq-mCherry, in order to confirm that patch clamped PC also expressed the excitatory DREADD, biocytin (7mg/mL, HelloBio #HB5035) was added to the intrapipette solution and slices were post-fixed overnight in 4% PFA. Slices were then washed and permeabilized before incubation with streptavidin conjugated-488 (ThermoFischer #S32354, 1/500) for 1h45. Post hoc confocal images (Leica SP8) of biocytin-filled PC and virally induced expression of mCherry were acquired to verify their colocalization.

Two-photon imaging

Acquisition

Ex vivo imaging of cerebellar slices were perfomed under a two-photon microscope (Femtonics, Budapest) equipped with an 8 kHz resonant scanner combined with a pulse laser (MaiTai-DS, SpectraPhysics, Santa Clara, CA, USA) tuned at 920 nm (green) or 1020 nm (red). Slices were continuously perfused with oxygenated ACSF (in mM: 110 NaCl, 5 KCl, 2.5 $CaCl_2$, 1.5 $MgSO_4$, 1.24 KH_2PO_4, 10 D-glucose, 27.4 $NaHCO_3$) and heated at 30-32°C using an automatic temperature controller (TC-324B, Warner Instruments). Images were acquired at 31.1 Hz. Typical imaging protocol consisted in ten minutes of baseline recording followed by fifteen minutes of treatment (e.g. CNO). For evoked NE-release, a stimulating electrode (borosilicate glass capillary from Phymep (1.5 OD x 0.86 ID x 100L) 2-3 MΩ) filled with ACSF was positioned in the molecular layer of the cerebellar cortex. Stimulation was delivered using a DS2A voltage stimulator - Mk.II (Digitimer) under software control, as a single train of 20 Hz. One stimulation was acquired prior to any treatment (baseline) and CNO was bath applied for 15 min before another train of stimulation without changing the position of the stimulating electrode. Calibration-curve protocols were acquired as followed: NE or DA was applied in increasing concentrations (in µM): 0, 0.01, 0.1, 0.25, 0.5, 1, for 3 min per concentration.

Analysis

Videos were exported in AVI format and averaged at 9 frames per second to reduce noise and improve signal quality. Analysis was performed using a custom-built Python pipeline called DETECT (Dynamic Extraction and Tracking of Emitted Cellular Transients) [3], specifically designed for an automatic, GMM-based (Gaussian Mixture Model) detection of spontaneous NE or GCaMP signals depending on the experiment. This pipeline identifies individual fluorescence clusters while correcting for background noise and motion correction. Following detection, we used TrackMate in Fiji (ImageJ) to extract a range of spatiotemporal features from each identified cluster, including area, perimeter, mean intensity, total number of events, and directionality of propagation. The resulting csv files were further processed and analyzed in MATLAB using custom-written scripts for group-level statistical comparisons and visualization. For evoked NE-release, videos were exported and treated in the same way, and stimulation response area and intensity was quantified with a custom-built matlab code. Calibration-curve data were extracted as above and analyzed with a custom-built python code where fluorescence movies were processed frame-by-frame. For each frame, the mean fluorescence of non-zero pixels was calculated to exclude static background, and $\Delta F/F$ was computed using the first 60 s of the drug-free period as F_0 to minimize bleaching effects. Traces were **smoothed** with a centered moving average. Pharmacological responses were quantified by fitting $\Delta F/F$ time courses with a four-parameter logistic model using nonlinear least-squares regression. Fits typically achieved R^2 values of ~0.92, and

parameter stability was confirmed by sensitivity analyses with 5% added noise. Baseline values were estimated over a 180 seconds pre-stimulation period.

Behavioral experiments

Treadmill-based locomotion assessment

To assess forced locomotion, WT and aVMAT2cKO mice were tested on a 5-lane treadmill (#8710RTS Panlab Harvard Apparatus). Both groups, WT and aVMAT2cKO mice, underwent the tamoxifen injections procedure. Each treadmill lane measured 532 mm in length, 100 mm in width and 50 mm in height. The treadmill was equipped with a control unit (LE8700TS Treadmill Control Unit, Panlab Harvard Apparatus) that allowed precise adjustment of speed parameters. The protocol, adapted from [4], starts with a stationary period (0 cm/s) for 1 minute, followed by an initial acceleration to 10 cm/s over 30 seconds. Mice were then maintained at 10 cm/s for three intervals: from 1.5 to 2 minutes, 3 to 4 minutes, and 5 to 6 minutes, each separated by 1 minute rest phases (0 cm/s). At 7 minutes, the speed was increased to 20 cm/s for 1 minute. The total duration of the protocol was 8 minutes.

Horizontal ladder test

To assess skilled locomotion and sensorimotor coordination, WT and aVMAT2cKO mice were subjected to the ladder rung walking test as previously described [5]. Both groups, WT and aVMAT2cKO mice, underwent the tamoxifen injections procedure. The apparatus consisted of two transparent plexiglass side walls (100 cm long, 20 cm high) and evenly spaced metal rungs (1 cm apart) forming a ladder elevated approximately 1 meter above the ground. Irregular sessions consisted of irregular spacing by randomly removing rungs in order to prevent pattern learning and challenge motor coordination. Each regular and irregular session consisted of 3 trials each. For irregular sessions, 3 random patterns were created and maintained identical for each mouse. Mice were familiarized to the task by performing 3 regular sessions prior to the tests. The following day, mice were tested with 3 regular sessions and 3 irregular sessions. They were placed at one end of the ladder and allowed to traverse to their home cage located at the opposite end. Crossings were recorded using a high-speed camera (200 fps, acA2040-120um, Basler Inc.) integrated into a custom closed-loop system that automatically adjusted the camera position to precisely track the mice as they traversed the ladder. The camera was positioned laterally and slightly inclined to capture precise paw movements. Videos were analyzed frame-by-frame (MPC software) to evaluate forelimb and hindlimb placements using a 7-points foot fault scoring system [5]:

- 0: correct placement
- 1: partial placement, paw is misplaced with only toes or heels
- 2: correction, paw aims for one rung but is placed on another without touching the first
- 3: replacement, paw position is adjusted after first initial placement
- 4: slight slip without fall
- 5: deep slip, paw slips leading to imbalance and fall
- 6: total miss, paw misses the rung leading to a fall.

For analysis, errors were expressed as a percentage of total steps to account for potential differences in step count across trials. The total number of errors per session and the corresponding error score intensity were measured.

$GRAB_{NE2h}$ miniscope imaging

To control for potential bias from the surgery or miniscope attachment on motor performances, mice performed the treadmill and horizontal ladder protocol before and after surgery for $GRAB_{NE2h}$ imaging. Imaging acquisition during the task was performed using the nVista miniscope system (Inscopix), fixed on the surgically implanted baseplate, with a 20 frames per second acquisition rate. Raw signals were then processed in Inscopix Data Processing Software as followed: after motion correction, regions of

interest (ROIs) were manually defined based on signal quality while avoiding blood vessels, using the same ROI size across videos. ΔF/F traces were then extracted and normalized for each ROI by their root mean square, and aligned to the behavioral videos for correlation analyses. Correlation analyses, power spectral density estimates, and statistical tests were performed in MATLAB.

Statistics

All data were analyzed using GraphPad Prism, MATLAB, and Python. Data normality was assessed using the Shapiro-Wilk test. Outliers were identified using the Robust Regression and Outlier Removal (ROUT) method (Q = 1%) [6] implemented in GraphPad Prism, which controls the false discovery rate, and were removed prior to statistical analysis. For comparisons between two groups, two-tailed paired or unpaired Student's t tests were used when data were normally distributed. Otherwise, the Wilcoxon signed-rank test (paired) or Mann-Whitney U test (unpaired) was applied. One- or two-way ANOVA, including repeated-measures designs where appropriate, were used, followed by post hoc multiple-comparison tests using Tukey's or Sidak's methods as appropriate. All data are reported as mean ± SEM. Statistical significance was set at $\alpha = 0.05$. *$p < 0.05$, **$p < 0.01$, ***$p < 0.001$ and ****$p < 0.0001$.

References

1. Petrelli, F. *et al.* Disruption of Astrocyte-Dependent Dopamine Control in the Developing Medial Prefrontal Cortex Leads to Excessive Grooming in Mice. *Biol. Psychiatry* **93**, 966–975 (2023).
2. Petrelli, F. *et al.* Dysfunction of homeostatic control of dopamine by astrocytes in the developing prefrontal cortex leads to cognitive impairments. *Mol. Psychiatry* **25**, (2020).
3. Niu, W. *et al.* Sharp and Fast Dynamic Extraction and Tracking of Emitted Cellular Transients. *bioRxiv* 2026.04.16.718018 (2026) doi:10.64898/2026.04.16.718018.
4. Paukert, M. *et al.* Norepinephrine controls astroglial responsiveness to local circuit activity. *Neuron* **82**, 1263–1270 (2014).
5. Metz, G. A. & Whishaw, I. Q. The ladder rung walking task: a scoring system and its practical application. *J. Vis. Exp.* https://doi.org/10.3791/1204 (2009) doi:10.3791/1204.
6. Motulsky, H. J. & Brown, R. E. Detecting outliers when fitting data with nonlinear regression - a new method based on robust nonlinear regression and the false discovery rate. *BMC Bioinformatics* **7**, (2006).

Extended data

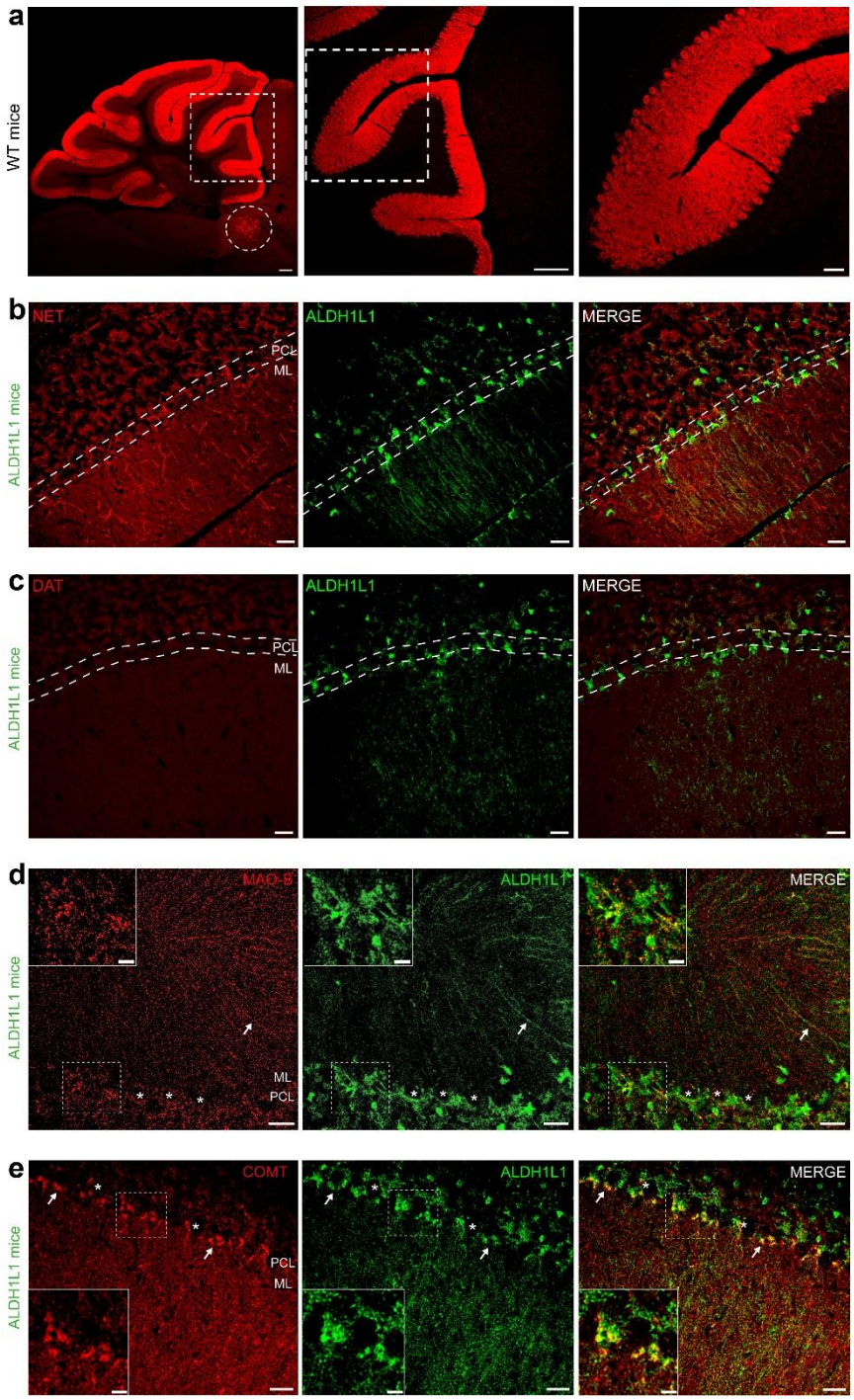

Figure 1. Monoaminergic signaling components in the cerebellar cortex. a. Tyrosine hydroxylase (TH, red) immunostaining in WT mice showing widespread labeling across cerebellar lobules. Dashed squares indicate regions shown at higher magnification (middle and right panels). The dashed circle highlights TH-positive *locus coeruleus* neurons (n = 8). Scale bar, 100 µm. **b.** NET immunostaining (red) in ALDH1L1-eGFP mice (green) showing NET expression restricted to sparse fibers within the molecular layer and absent from Bergmann glia (BG). Scale bar, 25 µm (n=4). Dashed lines delineate the Purkinje cell layer (PCL) and molecular layer (ML). **c.** DAT immunostaining (red) in ALDH1L1-eGFP mice (green) showing absence of DAT expression in the cerebellar cortex. Scale bar, 25 µm (n=2). Dashed lines delineate the Purkinje cell layer (PCL) and molecular layer (ML). **d.** MAO-B immunostaining (red) in ALDH1L1-eGFP mice (green) showing expression of monoamine degradation enzymes in BG. Insets show higher magnification views. Scale bars, 25 µm (main), 10 µm (inset) (n=2). **e.** COMT immunostaining (red) in ALDH1L1-eGFP mice (green) confirming expression of monoamine degradation pathways in BG. Insets show higher magnification views. Scale bars, 25 µm (main), 10 µm (inset) (n=3).

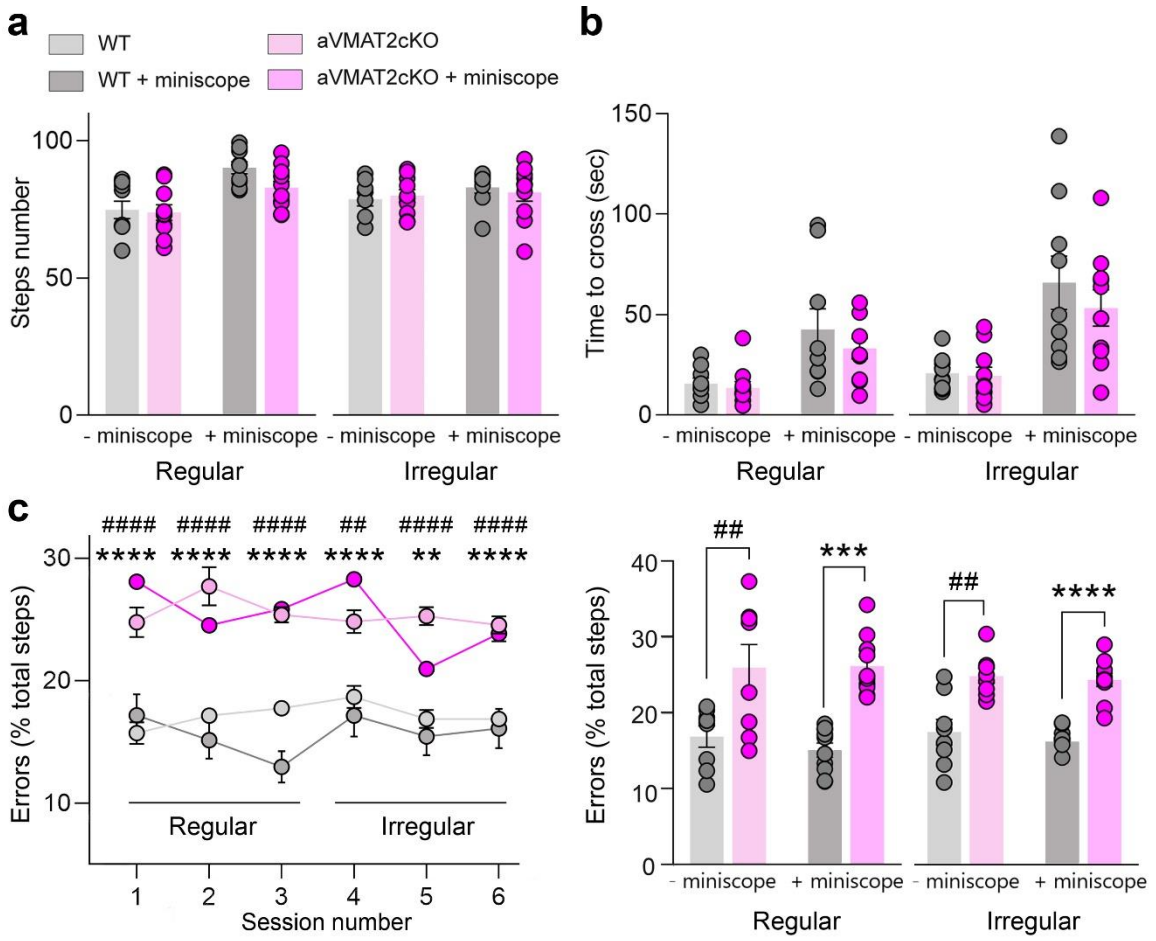

Figure 2. Horizontal ladder motor phenotypes are preserved after miniscope attachment. a. Total number of steps during ladder traversal in WT and aVMAT2cKO mice under regular and irregular conditions shows no genotype differences without (2-way ANOVA, regular p=0.99, irregular p=0.99) and with (2-way ANOVA, regular p=0.69, irregular p=0.71) miniscope. **b.** Time to cross the ladder is comparable between WT and aVMAT2cKO mice under both regular and irregular conditions, without (2-way ANOVA, regular p=0.99, irregular p=0.98) and with (2-way ANOVA, regular p=0.24, irregular p=0.96) miniscope. **c.** Left: Stepping error rate (% of total steps) across sessions under regular and irregular conditions. Right: Stepping error rates (% of total steps) are unchanged by miniscope attachment in both WT (2-way ANOVA, regular p=0.41, irregular p=0.12) and aVMAT2cKO mice (2-way ANOVA, regular p=0.685, irregular p=0.716). The increase in error rate in aVMAT2cKO remains significant without (2-way ANOVA, regular p=0.007, irregular p=0.0002), or with (2-way ANOVA, regular p=0.0002, irregular p<0.0001) miniscope. WT, n=9; aVMAT2cKO, n=10. Hash symbols (#) indicate genotype comparisons between WT and aVMAT2cKO mice without miniscope attachment, whereas asterisks (*) indicate genotype comparisons between WT and aVMAT2cKO mice with miniscope attachment. WT, n = 9; aVMAT2cKO, n = 10.

Supplementary video captions

Video 1. Detection of spontaneous NE transients in the cerebellar cortex. Left: Raw two-photon $GRAB_{NE2h}$ imaging showing spontaneous NE transients. Middle: Background removal using our custom pipeline (DETECT) (*10*), isolating spontaneous NE transients. Right: Detection and segmentation of NE transients for quantitative analysis. Scale bar, 25 µm. Displayed at 20x real-time speed.

Video 2. Extracellular Ca^{2+} removal abolishes spontaneous NE release. Left: Two-photon $GRAB_{NE2h}$ imaging of spontaneous NE transients under baseline conditions. Right: Two-photon imaging of spontaneous NE transients after extracellular Ca^{2+} removal. Scale bar, 25 µm. Displayed at 20x real-time speed.

Video 3. Chemogenetic silencing of LC noradrenergic neurons suppresses evoked NE transients in the cerebellar cortex. Left: Two-photons $GRAB_{NE2h}$ imaging of electrically evoked NE release in the molecular layer under baseline conditions. Right: Electrical stimulation after hM4Di chemogenetic silencing of LC noradrenergic neurons with CNO (10 µM, 30 min), showing suppression of evoked NE transients. Scale bar, 25 µm. Displayed at 20x real-time speed.

Video 4. Chemogenetic silencing of LC noradrenergic neurons does not abolish spontaneous NE release. Left: Two-photon $GRAB_{NE2h}$ imaging of spontaneous NE release under baseline ACSF conditions. Right: Two-photon $GRAB_{NE2h}$ imaging following chemogenetic silencing of LC noradrenergic neurons with CNO (10 µM, 30 min), showing persistent spontaneous NE release. Scale bar, 25 µm. Displayed at 20x real-time speed.

Video 5. Chemogenetic activation of Bergmann glia increases spontaneous NE release. Left: Two-photon $GRAB_{NE2h}$ imaging of spontaneous NE transients under baseline ACSF conditions. Right: Two-photon $GRAB_{NE2h}$ imaging during hM3Dq chemogenetic activation of Bergmann glia with CNO (10 µM), showing increased spontaneous NE transients. Scale bar, 25µm. Displayed at 20x real-time speed.

Video 6. Chemogenetic activation increases astroglial Ca^{2+} dynamics. Left: Two-photon GCaMP6f imaging of Bergmann glia Ca^{2+} transients under baseline ACSF conditions. Right: Two-photon GCaMP6f imaging during astroglial hM3Dq chemogenetic activation with CNO (10 µM), showing increased astroglial Ca^{2+} dynamics. Scale bar, 25 µm. Displayed at 5x real-time speed.

Video 7. Disruption of astroglial Ca^{2+} signaling reduces spontaneous NE transients and suppresses hM3Dq-induced increases in spontaneous NE release. Left: Two-photon $GRAB_{NE2h}$ imaging of spontaneous NE release under baseline ACSF conditions in mice expressing the calcium extruder CalEx in astroglial cells. Right: Two-photon $GRAB_{NE2h}$ imaging during chemogenetic activation of Bergmann glia with CNO (10 µM) in mice expressing CalEx in astroglial cells, showing suppression of the hM3Dq-induced increase in spontaneous NE release. Scale bar, 25 µm. Displayed at 20x real-time speed.

Video 8. CalEx suppresses astroglial Ca^{2+} dynamics during chemogenetic activation. Left: Two-photon GCaMP6f imaging of astroglial Ca^{2+} transients under baseline ACSF conditions in mice expressing the calcium extruder CalEx in cerebellar cortex astrocytes. Right: Two-photon GCaMP6f imaging during chemogenetic activation of Bergmann glia with CNO (10 µM) in mice expressing CalEx in astrocytes, showing reduced Bergmann glia Ca^{2+} dynamics. Scale bar, 25 µm. Displayed at 5x real-time speed.

Video 9. aVMAT2cKO mice show impaired motor coordination during the horizontal ladder task. Top: WT mouse performing the horizontal ladder task under irregular conditions. Bottom: aVMAT2cKO mouse performing the same task, showing increased fine and strong stepping errors. Displayed at 1x real-time speed.